Salas-Puente, RA.; Marzal-Romeu, S.; González-Medina, R.; Figueres Amorós, E.; Garcerá, G. (2018). An Algorithm for the Efficient Management of the Power Converters Connected to the DC Bus of a Hybrid Microgrid Operating in Grid-connection Mode. Electric Power Components and Systems. On line. https://doi.org/10.1080/15325008.2018.1469177

AN ALGORITHM FOR THE EFFICIENT MANAGEMENT OF THE POWER CONVERTERS CONNECTED TO THE DC BUS OF A HYBRID MICROGRID OPERATING IN GRID-CONNECTION MODE

Robert Salas-Puente*, Silvia Marzal, Raúl González-Medina, Emilio Figueres, Gabriel Garcerá.

Grupo de Sistemas Electrónicos Industriales del Departamento de Ingeniería Electrónica, Universitat Politècnica de València, Camino de Vera s/n, 46022 Valencia, España. Phone number: +34 963879606.

e-mail addresses: rosapue1@posgrado.upv.es (Robert Salas-Puente), silmarro@upv.es (Silvia Marzal), raugonme@upvnet.upv.es (Raúl González-Medina), efiguere@eln.upv.es (Emilio Figueres), ggarcera@eln.upv.es (Gabriel Garcerá).

**Corresponding author, e-mail address: rosapue1@posgrado.upv.es. Phone number: +34 963879606.*

Robert Salas-Puente was born in Merida, Venezuela, in 1981. He received the Ingeniero Electricista degree, in 2008 from the Universidad de Los Andes (ULA), Venezuela. He received the Ingeniería de Sistemas Electrónicos (M.Sc.) degree in 2015, from the Universitat Politècnica de València (UPV), Spain and he is currently working on his Ph.D. degree in the UPV. From 2009 he is working in the Electronics and Communications Department of the ULA, teaching in the electrical and electronical area. From 2013 he has been with the Electronics Engineering Department, UPV, where he is with the Industrial Electronic Systems Group (GSEI), http://gsei.upv.es. His main research fields are power converter modeling and control, integration and management of the distributed power sources in microgrids.

Silvia Marzal was born in Valencia, Spain, in 1984. He received the Ingeniero Telecomunicaciones (M.Sc) degree, in 2010 from the Universitat Politècnica de València (UPV), Spain and she is currently working on her Ph.D. degree studies on UPV, Spain. In 2012 he was with the Institute Center for Transportation and Territory on UPV, where she was involved in the design of communications systems applied to railway applications. From 2014, she has been with the Electronics Engineering Department, UPV, where she is with the Industrial Electronic Systems Group (GSEI), http://gsei.upv.es. Her main research fields are communications protocols and topologies design and development, to control and manage the distributed power sources in microgrids.

Raúl González-Medina was born in Valencia, Spain, in 1978. He received the Ingeniero Industrial (M.Sc.) degree in 2005 and the Dr. en Ingeniería Electrónica Ph.D. degree in 2015, from the Universitat Politècnica de València (UPV).
In 2005, he joined the Department of Electronics Engineering at the UPV, and got involved with the Industrial Electronic System Group (GSEI) where he is an R&D engineer, focused on technology transfer to companies. His main research fields are power converters, modulation techniques, grid-connected inverters, and converters for renewable energy sources.
Since 2015, he is also teaching power electronics in the Department of Electronic Engineering at the UPV.

Emilio Figueres received the M.Sc. degree from the Ecole Nationale Supérieure d'Electrotechnique, d'Electronique, d'Informatique et d'Hydraulique de Toulouse, Toulouse, France, in 1995, and the Dr. Ingeniero Industrial (Ph.D.) degree from the Universitat Politècnica de València (UPV), Valencia, Spain, in 2001. Since 1996, he has been with the Electronics Engineering Department, UPV, where he is currently a Full Professor and the Head of the Department. His main research interests include modeling and control of power converters, power processing of renewable energy sources, and grid connected converters for distributed power generation and improvement of power quality. In these fields, he has coauthored more than 100 papers published in JCR indexed journals and conferences. He also holds 3 patents and was a co-recipient of the best paper award published in 2012 in the IEEE Transactions on Industrial Electronics.

Gabriel Garcerá received the M.Sc. and Ph.D. degrees, both in Electrical Engineering, from the Universitat Politècnica de València (UPV) in 1993 and 1998, respectively. From 1993 to 1995 he was with the R&D Department of the company GH Group, involved in the design of switch-mode power supplies for particle accelerators at CERN. By the end of 1995 he joined the Electronics Engineering Department of the UPV, where he is currently a Full Professor. His main research fields are in power converter modeling and control, power supplies, power converters for renewable energy sources, microgrids and electric vehicles battery chargers. He is coauthor of more than 100 papers about power electronics in international journals and conferences. He has advised 13 Ph.D. Thesis. He was a co-recipient of the best paper award published in 2012 in the IEEE Transactions on Industrial Electronics (TIE). Since 2004, he is an Associate Editor of TIE.

AN ALGORITHM FOR THE EFFICIENT MANAGEMENT OF THE POWER CONVERTERS CONNECTED TO THE DC BUS OF A HYBRID MICROGRID OPERATING IN GRID-CONNECTION MODE

In this paper a centralized control strategy for the efficient power management of the power converters conforming a hybrid distributed generation microgrid is explained. The microgrid is based on a DC and an AC bus. The study is focused on the converters connected to the DC bus. The proposed power management algorithm is implemented in a microgrid central processor. This algorithm is based on assigning several operation functions to each of the generators, loads and energy storage systems in the microgrid. A communication system is used to assign the operation functions to each of the microgrid elements. The power flows between the DC and AC buses are studied in several operation scenarios, in which the proposed control can be verified.
Experimental and simulation results demonstrate that the algorithm allows to control the power dispatch inside the microgrid properly, by performing the following tasks: (1) the communications among power converters, the grid operator and intelligent loads, (2) the connection and disconnection of loads, (3) the control of the power exchange between the distributed generators and the energy storage system, (4) the compliance of the power dispatch limit set by the grid operator, (5) the synchronization with the grid and (6) the control of the voltage at the DC bus.

Keywords: Power management, microgrids, communications, energy storage systems, photovoltaics, power converters.

1. Introduction

Most countries are dependent on fossil fuels and nuclear energy for electric power generation. However, due to the increasing energy demand and the proliferation of new forms of energy generations which are cheaper and environment-friendly, many distributed generation (DG) systems have been integrated in the power grid [1]. Some DGs consist in Renewable Energy Sources (RES), such as: Photovoltaic (PV), wind, biomass, geothermal [2, 3]. The DGs are the basis of Microgrids (MGs), which can operate as a single power system that provides a safe and reliable operation at certain voltage and load levels [4]. A MG may work in island mode or in grid-connected mode, so that it can connect to DGs placed at various locations and inject their energy to the grid if needed [5]. There are three basic MG topologies, which can be classified according to the nature of their voltage: DC microgrid (DC MG) [6, 7], AC microgrid (AC MG) [8], and hybrid microgrid (HY MG), which is an MG with AC and DC buses. HY MGs are currently of great interest to researchers and are considered the distribution and transmission systems of the future, because they enable the coexistence of both AC MGs and DC MGs [9-11]. The main drawback of HY MGs is the large amount of complex power electronics interfaces required, that may complicate the control, management, communication and power dispatch among devices. Besides, the protection strategy of HY MGs is more complex than that of traditional MG [12, 13].

Early proposals for the control of an HY MG were shown in [9-11]. In [14] a decentralized control of a MG is proposed using an interlinking converter (ILC) in order to coordinate the power flows among the power converters connected to the AC and DC buses. Droop methods [15] were used to share the power delivered by the converters under operation. Droop was applied in [14] to the power converters connected both to the DC and to the AC bus. That control concept was extended in [16] and [17] to implement the power

interchange among the subgrids conforming a HY MG. Several studies about power management in HY MGs using droop strategies for the power dispatch have been recently presented [18]. In [19] the droop concept is extended in combination with a cost function defined for the power dispatch.

In that work a different approach to the power dispatch inside the HY MG is used, because a centralized control decides the status of the DGs, the loads and the energy storage system (ESS) in the MG by applying a set of predefined operation functions to each of the elements under operation. The approach of this paper is based on secure communications between the microgrid elements and a microgrid central processor (MGCP).
The main contributions of this manuscript are:

(1) The comprehensive design of a practical power management algorithm which is programmed inside an MGCP.
(2) The definition of a set of twelve operation functions for each of the microgrid elements: generators, loads and energy storage systems. Those functions are chosen by the MGCP in real time and broadcasted by the MGCP to the MG elements in order to set their status.
(3) The definition of hysteresis levels for the comparison with the power thresholds which determine a change of the functions to be applied to the MG elements.
(4) Compliance of the power dispatch limits established by the grid operator regarding the power flow between the HY MG and the public grid.
(5) The evaluation on an experimental platform of the proposed algorithm in several MG scenarios.

The MGCP sets the operation mode of each device connected to the HY MG by means of an RS485 serial communications system implemented on the MODBUS [20] protocol. MODBUS has a suitable performance in the MG environment [21], incorporating a cyclic redundancy code (CRC) to check the message integrity. A floating point TMS320F28335 DSP inside each of the power converters under operation has been used to implement the corresponding inner controllers. The power management algorithm has been implemented in an MGCP based on a TMS320F28335 DSP running at 150 MHz. This paper consists of 5 sections. After the introduction of section 1, in section 2 a general description of the HY MG under study is provided. In section 3 several concepts of the power management algorithm are explained, like its structure, system parameters, priority variables, limitations and the operation functions applied by the MGCP. In section 4 simulation and experimental results at different scenarios of the MG are presented. In section 5 the conclusions of the study are presented.

2. Description of the hybrid microgrid under study.

The proposed HY MG is depicted in Figure 1. The parameters of the communication system inside the MG are shown in Table 1. The nomenclature used in this paper is listed in Table 2. The HY MG under study is based on a single DC bus and a single AC bus, connected to the PCC of the public grid by means of a static switch. The connection of the DC and AC buses is performed by an ILC, allowing a bidirectional power flow. In grid connected mode the ILC may work as a current source that injects power to the grid synchronously with the AC bus voltage. The MGCP sets the operation functions of each of the power converters, loads and the ESS as a function of the MG scenarios. These scenarios depend on internal and external changes that affect the dispatchable power, such as changes

of the solar irradiation, of the load, of the power limit established by the public grid operator and of the ESS batteries state of charge (SOC).

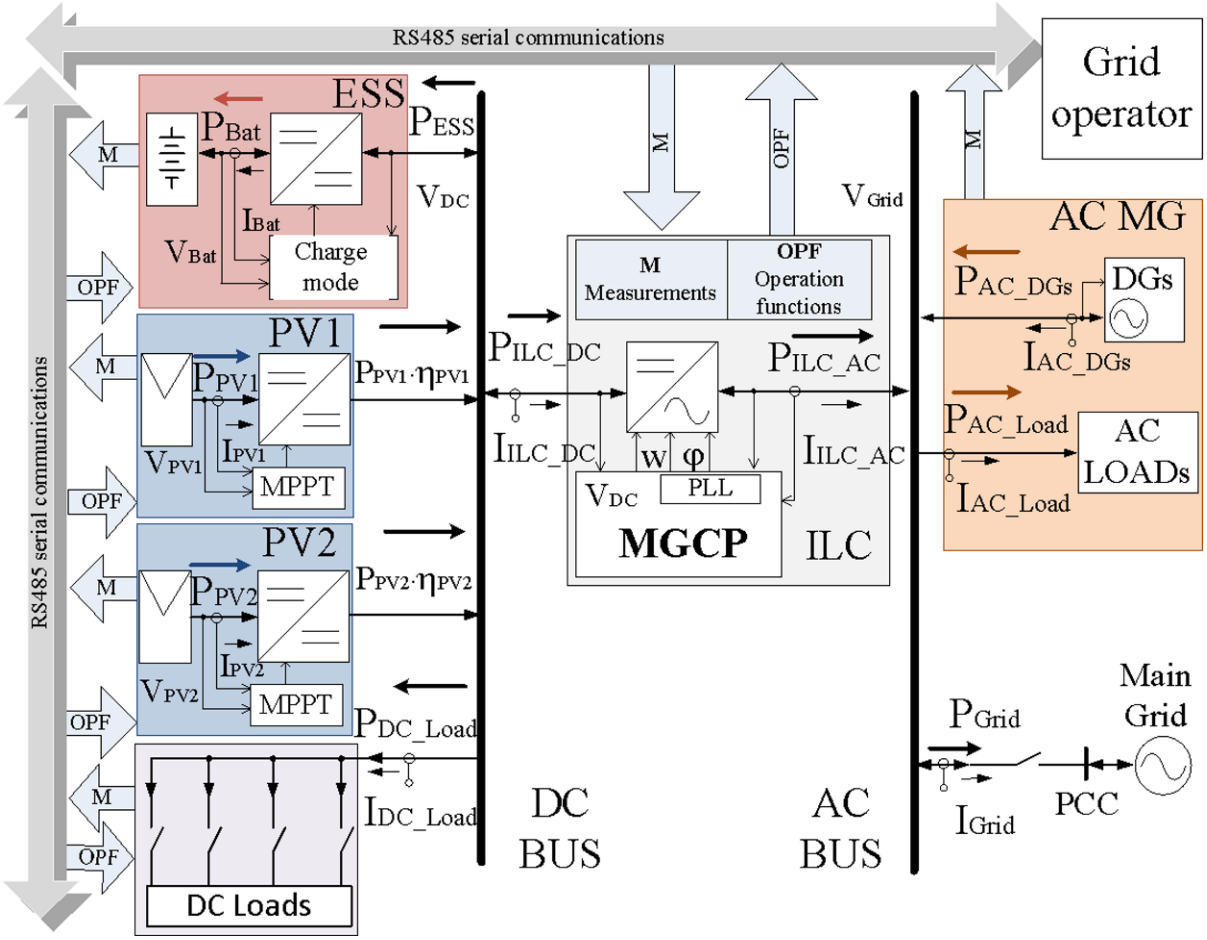

Figure 1. Conceptual scheme of the hybrid microgrid under study.

The MGCP achieves a suitable power dispatch by broadcasting several control actions to the microgrid devices: (a) connection/disconnection of the loads as a function of the generated power and the available energy stored in the batteries, (b) distribution of the available power between the critical loads and the ESS, (c) definition of hysteresis levels in the comparison with power thresholds which define a change of the operation mode of the MG elements, so that a stable DC bus voltage is obtained, and (d) compliance of the power limits established by the grid operator regarding power import/export from/to the public grid. Note that the grid operator can establish different power exchange limits in any moment by means of serial communications. Obviously, the power generated by the energy sources connected to the DC bus must be limited by the MGCP to prevent an excessive power injection to the public grid beyond the limit set by the grid operator.

The MGCP defines the internal functionality depending on the possible scenarios of the HY MG. The communications allow controlling the PV DGs, the ESS and the load connection/disconnection. In Figure 1 a 10 kW ILC, which connects the AC bus and the DC bus, can be observed. The AC bus is single phase and works in grid-connected mode with a grid voltage: $V_{Grid}=230\ V_{rms}$ and $F_{Grid}=50\ Hz\ \pm 1\ Hz$. In the HY MG under study two additional elements are connected to the AC bus: a 5 kW AC DG, and a 4 kW AC load. The nominal DC bus voltage is $V_{DC}=420\ V$, being regulated by the ILC. Three elements are connected to the DC bus: a 3 kW bidirectional DC-DC converter connected to a battery bank

and two 5 kW DC-DC converters connected each one to one PV array. The voltage at the battery bank (V_{Bat}) ranges from 192 V to 252 V, whereas the voltages at the PV arrays (V_{PV1} and V_{PV2}) vary from 306 V to 378 V. Additionally four 'shed-able' 2 kW DC loads are connected to the DC bus. The loads can be connected or disconnected to/from the DC-bus by means of individual switches controlled by the MGCP ($Sw1_{LoadDC}$ to $Sw4_{LoadDC}$).

Table 1. Communication parameters of the system

Communication parameters between the devices of the HY MG and the MGCP						
	DC MG				**AC MG**	
	ESS	**ILC**	**PV**	**Load**	**DGs**	**Load**
Operations functions	V_{DC_ref} I_{Dis_ref} I_{Ch_ref} VC Z_3	φ ω V_{DC_ref}	P_{PV_Lim}	$Sw_{1\_Load\_DC}$ $Sw_{2\_Load\_DC}$ $Sw_{3\_Load\_DC}$ $Sw_{4\_Load\_DC}$		
Measurements	I_{Bat} V_{DC} V_{Bat} SOC	I_{ILC_AC} V_{DC} V_{Grid}	I_{PV1} V_{PV1} I_{PV2} V_{PV2}	I_{DC_Load}	I_{AC_DGs} V_{Grid}	I_{AC_Load} V_{Grid}
Communication parameters between the MGCP and the grid operator						
High-level control			EDL, $\hat{P}_{\text{Grid-to-MG}}$, $\hat{P}_{\text{MG-to-Grid}}$			

3. Management and control of the HY MG

3.1 Parameters of the MGCP

In this section several concepts and parameters of the MGCP are explained, in order to define the features and control functionalities of the HY MG for the efficient application of the proposed algorithm.

3.1.1 High-level control limits

The main grid operator establishes a tertiary high-level control strategy which controls the power flow between the HY MG and the grid. That power flow imposes a limit of the power injected from the HY MG to the grid or vice versa. The limits from the high-level control are:

Energy Dispatch Limit (EDL)

EDL is a digital flag that tells the MGCP if there exists an energy dispatch limit in the MG. EDL allows the MGCP to set a suitable control strategy by taking into account the values of the maximum power extracted/injected from/to the grid to/from the HY MG. When *EDL=Off* there is no energy dispatch limit and the MGCP can inject or extract unlimited power to/from the grid. In the opposite case (*EDL=On*) the MGCP establishes a set of power

management criteria which depend on the load connected to the AC or DC buses, on the power available in the MG and on the SOC of the batteries.

Table 2. Nomenclature

P_{PV1}, P_{PV2}	Power supplied by the PV arrays 1 and 2
P_{PV}	PV power generated by the DC MG
P_{DCLoad}	Overall power consumed by the DC loads
P_{Grid}	Power injected from the HY MG to the grid
P_{ILC_AC}	Power injected from the DC bus to the AC bus by the ILC, measured at the AC side of the ILC
P_{ILC_DC}	Power injected from the DC bus to the AC bus by the ILC, measured at the DC side of the ILC
P_{ESS}	Battery bank charge power seen from the DC bus
P_{Bat}	Battery bank charge power
P_{ACLoad}	Overall power consumed by the AC loads
P_{AC_DGs}	Power supplied by the AC DGs
η_{EES}	Efficiency of the ESS
η_{PV1}, η_{PV2}	Efficiency of the PV DC-DC converters 1 and 2
η_{ILC}	Efficiency of the ILC
I_{Grid}	RMS Current injected from the HY MG to the grid
V_{Grid}	RMS value of the grid voltage
ω	Grid angular frequency
φ	Grid phase
I_{ACLoad}	Overall RMS current consumed by the AC loads
I_{DCLoad}	Overall current consumed by the DC loads
V_{DC}	DC bus voltage
I_{ILC_AC}	RMS current injected from the ILC to the AC bus
SOC	State of charge of the battery bank
I_{Bat}	Battery bank charge current
V_{Bat}	Battery bank voltage
I_{Ch_ref}	Reference of the battery charge current
I_{Dis_ref}	Reference of the battery discharge current
I_{PV1}, I_{PV2}	Current supplied by the PV arrays 1 and 2
P_{PV_Lim}	Required PV power limit
I_{DCLoad}	Overall current consumed by the DC loads
$S_{W1,2,3,4DC\_Load}$	DC load switches (load 1 to 4)
EDL	Energy dispatch limit
$\widehat{P}_{Grid\text{-}to\text{-}MG}$	Maximum power drawn from the grid to the HY MG
$\widehat{P}_{MG\text{-}to\text{-}Grid}$	Maximum power injected to the grid from the HY MG
$\widehat{P}_{ILC\_AC\|Grid\text{-}to\text{-}MG}$	Maximum power drawn from the AC bus to the DC bus measured at the AC side of the ILC
$\widehat{P}_{ILC\_AC\|MG\text{-}to\text{-}Grid}$	Maximum power injected from the DC bus to the AC bus measured at the AC side of the ILC
$P_{ILC\_AC\text{-}Rated}$	Rated power of the ILC measured at its AC side
$P_{ILC\_DC\text{-}Rated}$	Rated power of the ILC measured at its DC side
$\widehat{P}_{DC\_Load}$	Maximum power consumed by the DC loads
$P_{Available\_DCMG}$	Power available at the DC bus of the HY MG
DC_{Load_hyst}	DC load hysteresis
$PESS_{C10}$	Power drawn by the ESS from the DC bus at a battery charge current equal to C10

Maximum power extracted from the grid $\left(\hat{P}_{Grid\text{-}to\text{-}MG}\right)$

The power flow scenarios between the grid and the HY MG are shown in Figure 2. Two general cases are possible: $P_{Grid}<0$ and $P_{Grid}>0$, being the power flow from the grid to the microgrid or vice versa. Parameter $\hat{P}_{Grid\text{-}to\text{-}MG}$ is established by the grid operator, standing for the maximum power that can be extracted from the main grid to the HY MG, $|P_{Grid}|\leq\hat{P}_{Grid\text{-}to\text{-}MG}$.

Maximum power injected to the grid $\left(\hat{P}_{MG\text{-}to\text{-}Grid}\right)$

Parameter $\hat{P}_{MG\text{-}to\text{-}Grid}$ stands for the maximum power that can be injected from the HY MG to the main grid. This parameter is established by the grid operator, imposing condition $P_{Grid}\leq\hat{P}_{MG\text{-}to\text{-}Grid}$.

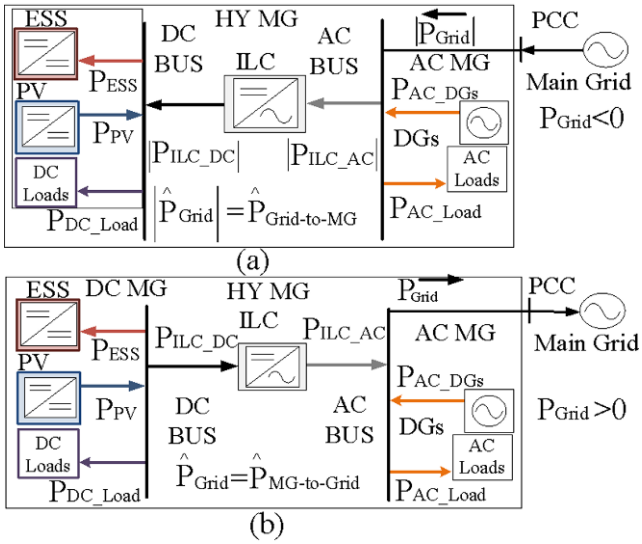

Figure 2. Power flow scenarios between the grid and the HY MG: (a) $P_{Grid}<0$, power flow from the Grid to HY MG and (b) $P_{Grid}>0$, power flow from the HY MG to Grid.

3.1.2 Parameters of the MGCP

The MGCP establishes some parameters for the secondary control strategy, which is responsible for the power flow between the AC bus and the DC bus of the HY MG. The MGCP must limit the power generated by the RESs, if the available power is higher than that necessary at the MG buses. The secondary control parameters are described in the following.

Maximum power extracted from the AC bus to the DC bus measured at the AC side of the ILC $\left(\hat{P}_{ILC_{AC}}|_{Grid\text{-}to\text{-}MG}\right)$

The power flow from the grid to the HY MG is depicted in Figure 2(a), in that situation the absolute value of P_{ILC_AC} can be calculated by (1), where $P_{Grid}<0$ and $P_{ILC\_AC}<0$. Parameter $\hat{P}_{ILC_{AC}}|_{Grid\text{-}to\text{-}MG}$ stands for the maximum power which can be extracted from the AC bus to the DC bus, measured at the AC side of the ILC, being given by (2). As the value of $\hat{P}_{Grid\text{-}to\text{-}MG}$ is set by the MGCP, the value of $\hat{P}_{ILC_{AC}}|_{Grid\text{-}to\text{-}MG}$ also depends on the MGCP. The maximum absolute value of P_{ILC_AC} must meet condition (3) at any time, taking into account the rated power of the ILC. In this study: $P_{ILC\_rated}=10\ kW$.

$$|P_{ILC_{AC}}| = P_{AC_{DGs}} + |P_{Grid}| - P_{AC_{Load}} \quad (1)$$

$$\widehat{P}_{ILC_{AC}}|_{Grid\text{-}to\text{-}MG} = P_{AC_{DGs}} + \widehat{P}_{Grid\text{-}to\text{-}MG} - P_{AC_{Load}} \quad (2)$$

$$|P_{ILC_{AC}}| \leq MIN\left(P_{ILC_{AC-Rated}}, \widehat{P}_{ILC_{AC}}|_{Grid-to-MG}\right) \quad (3)$$

Maximum power injected from the DC bus to the AC bus measured at the AC side of the ILC $\left(\widehat{P}_{ILC_{AC}}|_{MG\text{-}to\text{-}Grid}\right)$

The power flow from the HY MG to the grid is depicted in Figure 2(b), in that situation the value of P_{ILC_AC} can be calculated by (4), being $P_{Grid}>0$ and $P_{ILC\_AC}>0$. Parameter $\widehat{P}_{ILC_{AC}}|_{MG\text{-}to\text{-}Grid}$ stands for the maximum power which can be injected from the DC bus to the AC bus, measured at the AC side of the ILC, see (5). The maximum power injected from the DC bus to the AC bus by the ILC must meet condition in (6).

$$P_{ILC_{AC}} = P_{Grid} + P_{AC_{Load}} - P_{AC_{DGs}} \quad (4)$$

$$\widehat{P}_{ILC_{AC}}|_{MG\text{-}to\text{-}Grid} = \widehat{P}_{MG\text{-}to\text{-}Grid} + P_{AC_{Load}} - P_{AC_{DGs}} \quad (5)$$

$$\widehat{P}_{ILC_{AC}} \leq MIN\left(P_{ILC_{AC-Rated}}, \widehat{P}_{ILC_{AC}}|_{MG-to-Grid}\right) \quad (6)$$

PV power generated by the DC MG (P_{PV})

Parameter P_{PV} is the overall PV power generated by the DC MG. The powers generated by the PV DGs connected to the DC bus are measured individually. The total power generated by two PV DC-DC converters connected to the DC bus is shown by (7).

$$P_{PV} = P_{PV1} \cdot \eta_{PV1} + P_{PV2} \cdot \eta_{PV2} \quad (7)$$

Power consumed by the loads connected to the DC and AC buses

The powers consumed by the loads connected to the DC bus is $P_{DC_{Load}} = I_{DC_{Load}} \cdot V_{DC}$ and to the AC bus is $P_{AC_{Load}} = I_{AC_{Load_{rms}}} \cdot V_{Grid_{rms}}$.

Maximum power consumed by the loads connected to the DC bus $\left(\widehat{P}_{DC_{Load}}\right)$

Parameter $\widehat{P}_{DC_{Load}}$ stands for the maximum overall power which the DC loads is allowed to consume. The load shedding at the DC bus, performed by the MGCP, depends on this parameter. $\widehat{P}_{DC_{Load}} \leq P_{ILC_{DC\text{-}Rated}}$ establishes an upper limit for that maximum power as a function of the ILC power rating.

PV Power limit (P_{PV_Lim})

Parameter P_{PV_Lim} is the maximum power that should be extracted from the PV sources at any time, so that it can be consumed by the DC loads and by the batteries ($P_{ESS}>0$) and/or it injected to the grid. P_{PV_Lim} is represented by (8), where $P_{ESS} = (V_{Bat} \cdot I_{Bat})/\eta_{ESS}$.

$$P_{PV_{Lim}} = \widehat{P}_{ILC_{AC}}|_{MG\text{-}to\text{-}Grid} + P_{DC_{Load}} + P_{ESS} \quad (8)$$

PV Generation power available in the DC MG ($P_{Available\_DC\_MG}$)

Parameter $P_{Available\_DC\_MG}$ is the extra power available from the PV DGs making up the DC MG after feeding the load connected in the DC bus. The available PV generation power is defined in (9).

$$P_{Available_{DC\_MG}} = P_{PV} - P_{DC_{Load}} \quad (9)$$

DC load switch

The DC load switch flag takes two possible states, $SW_{LoadDC}=ON$ and $SW_{LoadDC}=OFF$, depending on the connection or disconnection of loads to the DC bus, respectively.

DC load hysteresis (DC_{Load_hyst})

Parameter DC_{Load_hyst} is calculated as 10% of the overall power consumed by the DC loads, $DC_{Load_{hyst}} = 01 \cdot P_{DC_{Load}}$. This parameter acts as a hysteresis value for the comparison thresholds which produce the decisions of the MGCP, so that undesirable power transients are avoided.

Power consumed for the batteries to C10 ($PESS_{C10}$)

Parameter $PESS_{C10}$ is the maximum power consumption for the charge of the batteries of the ESS, $PESS_{C10} = (V_{Bat} \cdot I_{C10})/\eta_{ESS}$. It has been established that the batteries are charged with a current equal to $I_{C10} = C_{10}/10$, being $C10$ the specified battery capacity (measured in A·h) for a discharge time of 10 hours.

3.2 HY MG management algorithm

Several calculations and functions are necessary for the decision-making of the HY MG control algorithm. These calculations and functions depend on the SOC of the battery, the availability of power in the buses, the limits set at a higher level, and the status of SW_{LoadDC}.

3.2.1 Operation functions the MGCP

The power management algorithm embedded in the MGCP executes 12 operation functions according to the various operating scenarios. The operation functions of the MGCP and their interactions with the converters of the MG are described in the following.

3.2.1.1 Operation functions in DC load connection mode ($SW_{LoadDC}=ON$)

Function 1 (F1): Function F1 establishes that DC loads are fed. While $SOC \leq SOC_{Full}$, the DC-DC converter of the ESS charges the batteries from the DC bus with a current I_{C10}. The PV DGs work at their maximum power point (MPP), so that $MPPT=ON$. If there´s not enough power available from the PV DGs connected to the DC bus, the ILC can extract the rest of the power from the AC bus with the only restriction: $|\widehat{P}_{ILC_{AC}}| \leq P_{ILC_{AC\text{-}Rated}}$, taking into

account that *EDL=OFF*.

Function 2 (F2): All DC loads are fed. While $SOC \leq SOC_{Full}$, the DC-DC converter of the ESS charges the batteries from the DC bus with a current equal to I_{C10}. The PV DGs work at their MPP (*MPPT=ON*). In this case the PV DGs connected to the DC bus may produce an excess of power which can be injected to the AC bus by the ILC, with the only limitation of its rated power, $\widehat{P}_{ILC_{AC}} \leq P_{ILC_{AC\text{-}Rated}}$, if is necessary.

Function 3 (F3): All DC loads are fed. While $SOC \leq SOC_{Full}$, the DC-DC converter of the ESS charges the batteries from the DC bus with a current equal to I_{C10}. The PV DGs don´t work at their MPP (*MPPT=OFF*). In this case the PV DGs connected to the DC bus produce a limited amount of power, because the power which can be injected to the AC bus by the ILC is limited by the grid operator. The power injected from the DC bus to the AC bus by the ILC is given by: $P_{ILC_{AC}} \leq \widehat{P}_{ILC_{AC}}|_{MG\text{-}to\text{-}Grid}$. Figure 3 depicts the power dispatch inside the HY MG after applying the operation functions F3, F8, F10 and F11. Function 3 is shown in Figure 3(a).

Function 4 (F4): All DC loads are disconnected. $SOC \leq SOC_{MIN}$, the ESS is in standby mode. The flag SW_{LoadDC} changes from ON to OFF, entering the DC load disconnection mode. The PV DGs work at their MPP (*MPPT=ON*).

Function 5 (F5): All DC loads are fed. While $SOC \leq SOC_{Full}$, the DC-DC converter of the ESS charges the batteries from the DC bus with a current equal to I_{C10}. The PV DGs work at their maximum power point (*MPPT=ON*). The ILC injects the excess power at the DC bus to the AC bus. The power injected to the AC bus must comply: $P_{ILC_{AC}} \leq \widehat{P}_{ILC_{AC}}|_{MG\text{-}to\text{-}Grid}$.

Function 6 (F6): All DC loads are fed. As the SOC has reached SOC_{Full}, the DC-DC converter of the ESS stops charging the batteries, setting the ESS in standby mode. The PV DGs work at their MPP (*MPPT=ON*), producing an excess of power which can be injected to the AC bus by the ILC.

Function 7 (F7): All DC loads are fed. While $SOC \leq SOC_{Full}$, the DC-DC converter of the ESS charges the batteries from the DC bus with a current, whose value is shown by (10), which is smaller than I_{C10}. The PV DGs work at their MPP (*MPPT=ON*). If there´s not enough power available from the PV DGs, the ILC can extract the rest of power from the AC bus, subjected to the limit: $|P_{ILC_{AC}}| \leq \widehat{P}_{ILC_{AC}}|_{Grid\text{-}to\text{-}MG}$.

$$I_{Ch_{ref}} = MIN\left(I_{C10},\ \frac{P_{Available_{DC\_MG}} + \hat{P}_{ILC_{AC}}|_{Grid-to-MG}}{V_{DC}}\right) \quad (10)$$

Function 8 (F8): All DC loads are fed. While $SOC \geq SOC_{MIN}$ the DC-DC converter of the ESS operates as a controlled current source discharging the batteries to the DC bus. In F8 the PV DGs work at their MPP (*MPPT=ON*). The sum of the power coming from the ESS and from the PV DGs is not enough to energize the DC loads, so that the required extra power can be transferred from the AC bus to the DC bus through the ILC. That extra power is limited in order not to override the power which can be absorbed by the DC loads. Equation (11) shows the expression of the discharge current. In this case the extra available power is negative ($P_{AvailableDC\_MG} < 0$), because the power coming from the PV DGs is not enough to energize the DC loads, see Figure 3(b).

$$I_{Dis_{ref}}=MIN\left(I_{C10},\ \left|\frac{P_{Available_{DC\_MG}}+\hat{P}_{ILC_{AC}}|_{Grid\text{-}to\text{-}MG}}{V_{bat}}\right|\right) \quad (11)$$

Function 9 (F9): All DC loads are fed. As the SOC has reached SOC_{Full}, the DC-DC converter of the ESS stops charging the batteries, entering standby mode. The PV DGs don´t work at their maximum power point (*MPPT=OFF*), because the DC loads cannot absorb the sum of MPP powers. The ILC injects a limited amount of power from the DC bus to the AC bus, which is the required extra power to feed the DC loads.

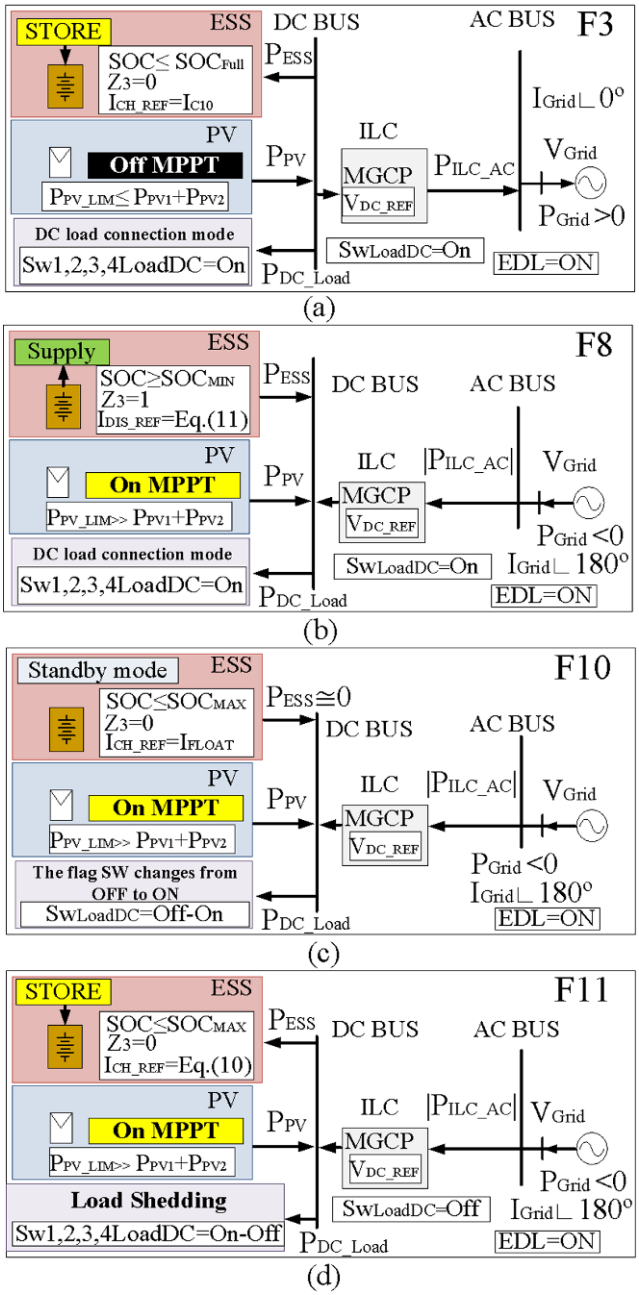

Figure 3. Power dispatch inside the HY MG after applying the operation functions: (a) Function 3, (b) Function 8, (c) Function 10 and (d) Function 11.

3.2.1.2 Operation functions in DC load disconnection mode (SW_{LoadDC}=OFF)

Function 10 (F10): In F10 the flag SW_{LoadDC} switches from OFF to ON. All DC loads are fed. The ESS is in standby mode. The PV DGs work at their MPP (*MPPT=ON*), function 10 is shown in Figure 3(c).

Function 11 (F11): Only some DC loads are fed (load shedding). This function selects the overall amount of power consumed by the DC loads. F11 offers the ability to turn on and turn off each of the DC loads automatically. While $SOC \leq SOC_{MAX}$, the DC-DC converter of the ESS charges the batteries with a current smaller than I_{C10}, given by (10). The PV DGs work at their MPP (*MPPT=ON*), function 11 is shown in Figure 3(d).

In equation (12) gives the expression of *Cal.0*, which is the calculation of the available PV power plus the maximum power that can be transferred from the AC bus to the DC bus by the ILC. A decision tree can be observed in Figure 4, which depicts how 1 to 4 DC-loads are connected-disconnected as a function of the value of *Cal.0*. If *Cal.0* is not enough to energize all the DC loads, F11 begins their disconnection depending on the values of *Cal.0* and of the state (1 or 0) of the logic variables *Comp.1* to *Comp.3*, which are calculated as OR functions. Note that a 10% hysteresis band of the power of one DC load has been chosen for establishing the comparison thresholds: $DC_{Load\_hyst}=0.1 \cdot 2\ kW=200\ W$.

$$Cal.0 = P_{PV} + \widehat{P}_{ILC_{AC}}|_{Grid\text{-}to\text{-}MG} \tag{12}$$

Function 12 (F12): All DC loads are fed. While $SOC \leq SOC_{MAX}$, the DC-DC converter of the ESS charges the batteries with a current smaller than I_{C10}, given by (10). The PV DGs work at their MPP (*MPPT=ON*). If the power coming from the PV DGs is not enough to energize the DC loads, the required extra power can be transferred from the AC bus to the DC bus through the ILC.

3.2.2 Power Management algorithm of the HY MG

Figure 5 depicts the flowchart of the proposed HY MG power management algorithm, *Comp.4* is a logic variable which is calculated as an OR function. The DC load switch flag, SW_{LoadDC}, and the flag *EDL*, are fundamental parameters for decision-making. When *EDL=Off*, there is no energy dispatch limit, so that functions F1 or F2 can be applied. When *EDL=On* and $SW_{LoadDC}=ON$, the MGCP applies functions F3 to F9. The flag SW_{LoadDC} can be turned off by F4, after which the MGCP can apply functions F10 to F12. The functions are implemented so that the power transfer limits between both buses are not exceeded. The basic calculations performed by the power management algorithm, *Cal.0* to *Cal.4*, are shown by (12) to (15), and allow checking the power availability of both buses, taking into account their power dispatch limits. Equation (13) stands for the power availability in the DC bus, coming from DGs and batteries, plus the maximum power which can be extracted from the AC bus to the DC bus.

$$Cal.1 = P_{Available_{DCMG}} + \widehat{P}_{ILC_{AC}}|_{Grid\text{-}to\text{-}MG} \tag{13}$$

Equation (14) stands for the maximum power which can be injected from the DC bus to the AC bus plus the power consumed for charging the batteries at a current I_{C10}.

$$Cal.2 = \widehat{P}_{ILC_{AC}}|_{MG\text{-}to\text{-}Grid} + P_{ESS_{C10}} \tag{14}$$

In equation (15) the maximum power consumed by the DC loads is extracted from the PV power generated at the DC bus plus the maximum power which can be extracted from the AC bus to the DC bus.

$$Cal.3 = P_{PV} + \widehat{P}_{ILC_{AC}}|_{Grid\text{-}to\text{-}MG} - \widehat{P}_{DC_{Load}} \quad (15)$$

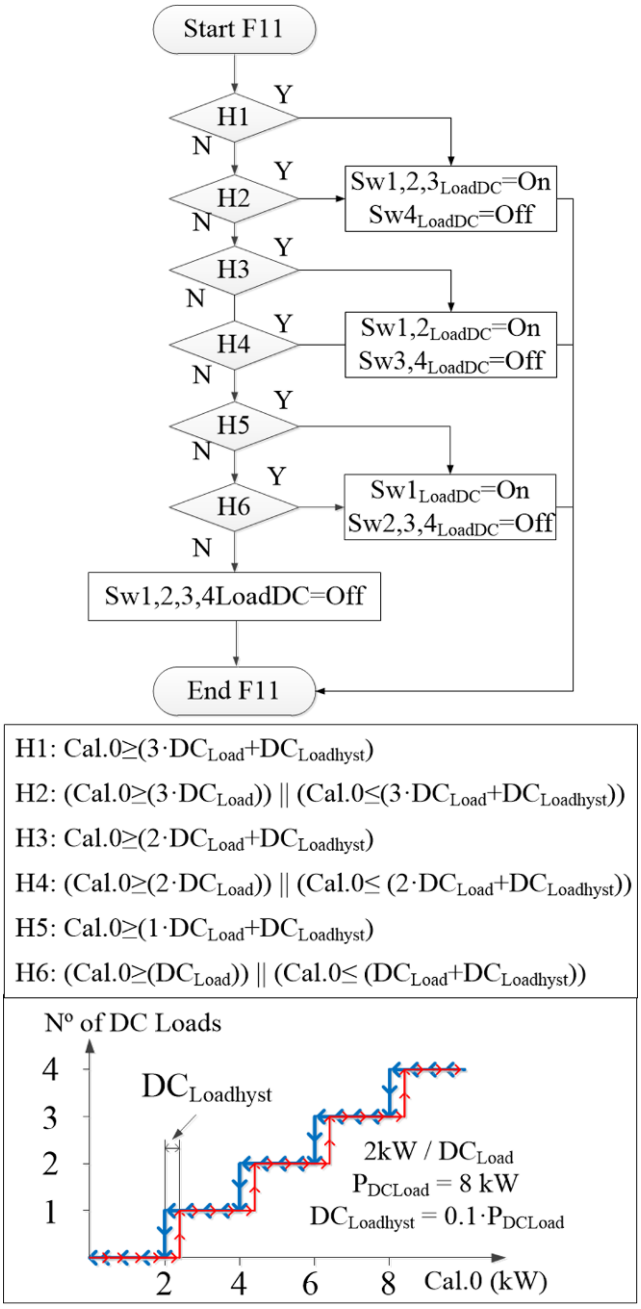

Figure 4. DC load shedding function.

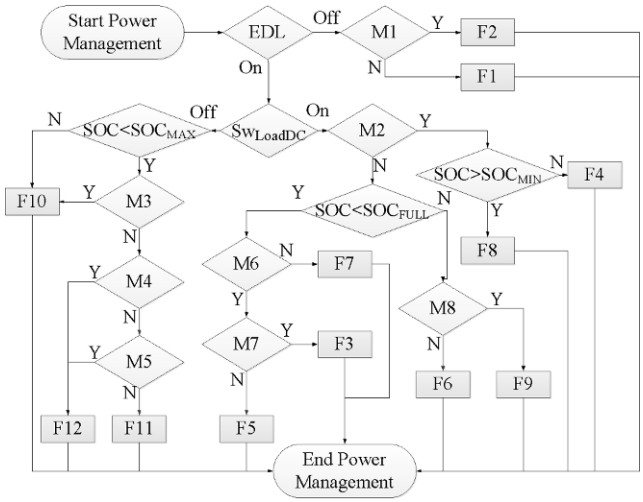

M1: $P_{AvailableDCMG}>0$
M2: $Cal.1>DC_{Loadhyst}$
M3: $Cal.3>DC_{Loadhyst}$
M4: $Cal.0\geq P_{DCLoad}$
M5: $Cal.0\leq(P_{DCLoad}+DC_{Loadhyst})$
M6: $Cal.1>PESS_{C10}$
M7: $P_{AvailableDCMG}>Cal.2$
M8: $P_{AvailableDCMG}>P_{ILCAC|MG\text{-}to\text{-}Grid}$

Figure 5. Power management algorithm of the HY MG.

4 Simulation and experimental results and discussion

4.1 Simulation results

The proposed power management algorithm has been simulated by means of PSIM™ [22] under various scenarios. This study is focused in the particular case that the MG is operating in grid connected mode. The characteristics of the power electronic converters composing the MG are listed in Table 3. The simulation scenarios of the MG are explained in Table 4. It is supposed that the ESS is initially discharged ($SOC\leq SOC_{MIN}$). A selected number of possible scenarios has been studied in order to demonstrate the suitable behavior of the HY MG in its most common and critical situations. In the scenarios under study step changes of the irradiation, of the DC load and of the *EDL* are considered, as it can be observed from Table 4. The behavior of the proposed algorithm and the application of particular functions F1 to F12 by the MGCP can be observed from the following graphs. Figure 6 depicts the behavior of the currents I_{Bat}, $I_{PV} = I_{PV1} + I_{PV2}$ and of the SOC with time. The evolution of the powers P_{Bat}, P_{PV}, P_{DCLoad}, P_{ILC_AC} and P_{Grid} can be observed from Figure 7. Figure 8 provides a detail of the strongest transient of I_{ILC_AC}, V_{DC} and P_{ILC_AC} which takes place in the whole simulation, corresponding to the time span 34.8 s to 35.4 s. The analysis is performed according to the following time intervals:

Interval 1 ($0\leq t < 1$ s): This interval is divided into 2 subintervals.

$0 \leq t < 40$ ms: At *$t=0$ s* the ESS is initially discharged ($SOC\leq SOC_{MIN}$). The irradiation is 300 W/m^2 and the overall DC load absorbs 8 kW. Due to the fact that the PV available power, P_{PV}, at that low irradiation level is not enough to feed the loads, the MGCP applies function F4, internally activating flag $SW_{LoadDC}=OFF$.

40 ms≤t< 1 s: After to F4, F11 is applied to disconnect two DC loads (overall *DC load=4 kW*) and the batteries are charged with a current given by (10).

Table 3. Characteristics of the power converters conforming the HY MG.

ILC	**2 PV DC-DC converters (DGs)**	**ESS**
P_{ILC}=10 kW V_{Grid}=230 V F_{Grid}=50 Hz V_{DC}=420 V F_{SW_ILC}=12.8 kHz C_{DC}=3.8 mF L1=1.8 mH L2=0.4 mH C=2 µF C_{DC}=3.8 mF	P_{PV_BOOST} =5 kW V_{PV}=306 V F_{SW_PV}=16 kHz Co_{PV}=1 mF Ci_{PV}=1 mF L_{PV}=5.4 mH **PV Panel: Atersa A-250P GSE** V_{PV_OC}=37.61 V I_{PV_MAX}=8.18 A V_{PV_MAX}=30.58 V I_{PV_CC}=8.71 A	P_{ESS_HB}=3 kW V_{Bat}=216 V F_{SW_ESS} =16 kHz Ci_{Bat}=1 mF Co_{Bat}=1 mF L_{Bat}=5.4 mH **Battery Bank: SUN POWER VRM 12V105** V_{Bat_NOM}=12 V V_{Bat_MIN}=10.28 V V_{Bat_MAX}=14.1 V C_{10}=105 A·h I_{C10}=10.5 A

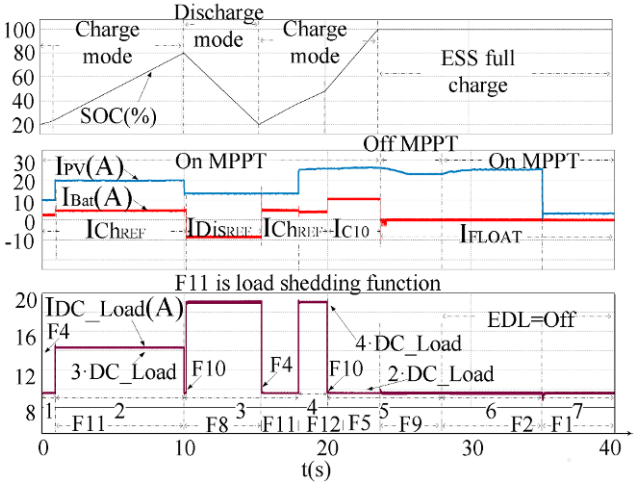

Figure 6. Evolution of the currents of the HY MG and of the SOC of the batteries.

Interval 2 (1 s ≤ t < 10 s): At *t= 1 s* the irradiation undergoes a change from 300 W/m^2 to 600 W/m^2, whereas the SOC keeps growing below SOC_{MAX}. The MGCP goes on applying F11. The PV generation is increased, and F11 connects an additional 2 kW DC load (overall *DC load=6kW*) to the DC bus. The MGCP makes both PV DC-DC converters to operate at their MPP, whereas the DC bus voltage is regulated to 420V by the ILC.

Interval 3 (10 s ≤t ≤18 s): This interval is divided into 5 subintervals.

10 ≤t < 10.2 s: At *t=10 s* the irradiation decreases from 600 W/m^2 to 400 W/m^2, whereas the SOC keeps growing below SOC_{MAX}. The MGCP maintains F11. The power generated by the panels P_{PV} with this irradiation is insufficient to feed three loads and F11 disconnects one load (*DC load=4kW*) in the DC bus. This is shown in Figure 6.

10.2 s ≤t <10.24 s: At *t=10.2 s* the SOC surpasses SOC_{MAX}, whereas the irradiation stays at a

constant value of 400 W/m^2. The MGCP applies F10 after detection of SOC_{MAX}, which internally activates the flag SW_{LoadDC}=*ON*.

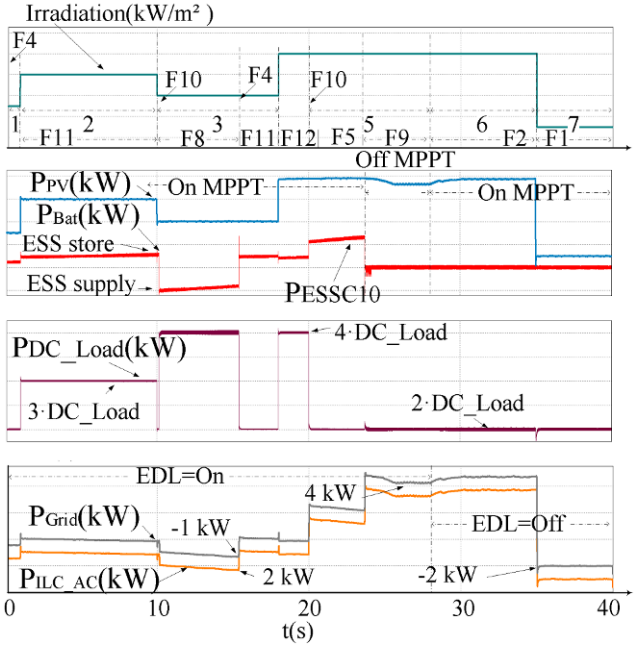

Figure 7. Evolution of the power exchange at the HY MG and irradiation.

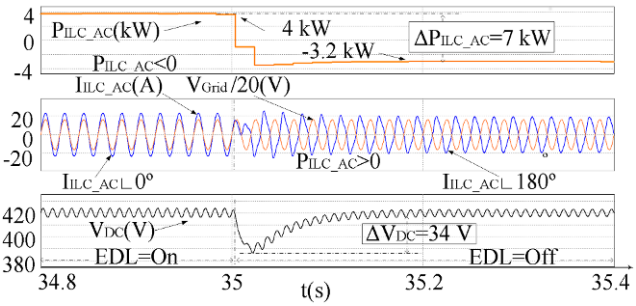

Figure 8. Detail of the strongest transient of I_{ILC_AC}, V_{Grid}, V_{DC} and P_{ILC_AC}, which takes place in interval 7.

10.24 s ≤ t <15.4 s: At *t=10.24 s* the generated PV power at the current irradiation level is not enough to feed all the DC loads, so that the MGCP applies F8 in order to get additional power from the ESS, and the battery bank is discharged at a current given by (11). F8 connecting all DC loads (8 kW) to the DC bus and extracts power from the AC bus taking into account the limit the maximum power that can be extracted of the same $|P_{ILC_{AC}}| \leq \widehat{P}_{ILC_{AC}}|_{Grid\text{-}to\text{-}MG}$, and the ESS injects the current required by the DC bus to feed the DC loads.

15.4 s ≤ t < 15.44 s: At *t=15.4 s* the SOC goes below SOC_{MIN}, so that the MGCP applies F4, internally activating flag SW_{LoadDC}=*OFF*.

15.44 s ≤ t < 18 s: At *t=15.44 s* the MGCP applies F11. F11 disconnects two DC loads (overall *DC load=4kW*), so that the batteries are charged with a current given by (10).

Interval 4 (18 s ≤ t < 20 s): At *t=18 s* the irradiation undergoes a linear change of 400 W/m^2

to 800 W/m^2, being $SOC<SOC_{MAX}$. The generated PV power and the power extracted from the AC bus are enough to feed all DC loads. Due to limitations on the amount of power that can be interchanged between the buses, the MGCP applies F12 and the batteries are charged with a current given by (10). F12 connects all the DC loads and also sets the PV sources at their MPP.

Table 4. Possible scenarios of the HY MG.

SIMULATION scenarios [(1)]							
Time intervals (s)							
Time interval number	1	2	3	4	5	6	7
Time span (s)	0<t<1	1<t<10	10<t<18	18<t<20	20<t<28	28<t<35	35<t<40
Irradiation (W/m^2)	300	600	400	800	800	800	100
Load connected at the DC bus	4 loads (8 kW)	4 loads (8 kW)	4 loads (8 kW)	4 loads (8 kW)	2 loads (4 kW)	2 loads (4 kW)	2 loads (4 kW)
EDL	On	On	On	On	On	Off	Off
ILC	The HY MG is operating in grid-connection mode						
ESS	The batteries of the ESS are initially discharged. $SOC \leq SOC_{MIN}$						
Power limits	$P_{MG\text{-}to\text{-}Grid}=4\ kW$, $P_{Grid\text{-}to\text{-}MG}=1\ kW$, $P_{DC\_LOAD}=8\ kW$						
AC MG	$P_{AC\_DG}=5\ kW$, $P_{AC\_LOAD}=4\ kW$						
[(1)] It´s worth pointing out that step changes of irradiation not correspond to reality, but they allow studying the behavior of the HY MG and the stability of the buses in the worst cases. In order to check of the proposed algorithm in different situations and for a short time period, in this work the algorithm is running in simulations at 25Hz. The duration of operation functions F4 and F10 is one clock cycle (40 ms), because their main function is to change the load shedding function.							
EXPERIMENTAL scenarios							
ESS	Experiment 1: The batteries of the ESS are initially charged. $SOC=SOC_{MAX}$						
Time span (s)	0<t<8	8<t<11	11<t<41	41<t<44	44<t<50		
Irradiation (W/m^2)	100	100 to 800	800	800 to 100	100		
ESS	Experiment 2: The batteries of the ESS are initially discharged. $SOC \leq SOC_{MIN}$						
Time span (s)	0<t<7	7<t<10	10<t<40	40<t<43	43<t<50		
Irradiation (W/m^2)	100	100 to 800	800	800 to 100	100		
DC Load connected	4 loads (2.4 kW)						
EDL	On						
ILC	The HY MG is operating in grid-connection mode						
Power limits	$P_{MG\text{-}to\text{-}Grid}=4\ kW$, $P_{Grid\text{-}to\text{-}MG}=1\ kW$, $P_{DC\_LOAD}=2.4\ kW$						
AC MG	$P_{AC\_DG}=5\ kW$, $P_{AC\_LOAD}=4\ kW$						

Interval 5 ($20\ s \leq t < 28\ s$): This interval is divided into 3 subintervals.

$20 \leq t < 20.04\ s$: The irradiation keeps a constant 800 W/m^2 value, whereas SOC remains below SOC_{Full}. At *$t=20\ s$* the load connected to the DC bus decreases from 8 kW to 4kW. The PV generated power (P_{PV}) at the current irradiation is enough to feed all DC loads. The MGCP applies F10 which internally activates the flag $SW_{LoadDC}=ON$.

$20.04 \leq t < 23.7\ s$: At *$t=20.04\ s$* MGCP applies F5. F5 sets the charge the batteries with a current I_{C10}. The PV sources work at their MPP. The ILC injects the power excess to the AC bus.

$23.7\ s \leq t < 28\ s$: Both the irradiation (800 W/m^2) and the DC load (4 kW) remain constant, whereas the SOC has reached 100%. The power generated by the panels is higher than that

necessary for feeding the DC loads, $P_{PV} > 4\ kW$. The MGCP applies F9 to stop charging the batteries and to set the PV generators outside their MPP (*MPPT=OFF*). In this case: $P_{ILC_{AC}} \leq \widehat{P}_{ILC_{AC}}|_{MG\text{-}to\text{-}Grid}$.

Interval 6 ($28\ s \leq t < 35\ s$): The irradiation and the SOC remain constant, 800 W/m^2 and 100%, respectively. EDL switches from On to Off. The MGCP applies F2 and the ILC injects power to the grid to its rated power if is necessary, $P_{ILC_{AC}} \leq P_{ILC_{AC\text{-}Rated}}$. At $t=30\ s$ MPPT switches from OFF to ON.

Interval 7 ($35\ s \leq t < 40\ s$): The irradiation undergoes a change of 800 W/m^2 to 100 W/m^2. The MGCP applies F1, so that the ILC can extract power from the grid, $|P_{ILC_{AC}}| \leq P_{ILC_{AC\text{-}Rated}}$. *MPPT=ON*.

In Figure 7 the power exchange between devices of the MG is shown. In the first part of interval 5 (20<t<23.7 s) the MGCP makes that the battery system is charged to its maximum capacity, $PESS_{C10}$, using the power available from the PV DGs. In the second part of interval 5 ($23.7\ s \leq t < 28\ s$) the MGCP limits the generation from the PV DGs, setting their operation point out of the MPP (*MPPT=OFF*).

The ILC is responsible for controlling the voltage of the DC bus, because the AC bus works in grid connection mode. The ILC also carries out the synchronization of the AC bus with the grid, achieving that the current I_{ILC_AC} flowing through the ILC to the AC bus is low distorted and in phase with the grid voltage, V_{Grid}, when the MG exports power to the grid or in phase opposition when the MG imports power from the grid. Figure 8 shows the waveforms of I_{ILC_AC} and of V_{Grid} in both situations, where a smooth transient, good synchronization and a low distortion of I_{ILC_AC} can be observed in the transition from exporting to importing power to/from the AC bus. A smooth transient of the DC bus voltage, V_{DC}, is also observed in that transition at $t=35$ s, which is the strongest transient of the DC bus during the whole study, consisting of a transient undervoltage of $\Delta\widehat{V}_{DC}=34\ V$, less than 10% of the DC bus voltage. It should be considered that the power, P_{ILC_AC}, interchanged between the ILC and the AC bus at $t=35\ s$ undergoes an abrupt change from 3.8 kW to -3.2 kW (7 kW step), provoked by a fast irradiation decrease.

4.2 Experimental results.

Several experimental power electronic converters, whose characteristics are summarized in Table 3, have been built for validating the proposed power management algorithm. The following devices have been connected to the DC bus of the HY MG available in the lab: a 3 kW battery ESS, a 2.5 kW PV source and four electronic switches to connect/disconnect four DC loads of 600 W each one ($\widehat{P}_{DC\_Load} = 2.4\ kW$). Figure 9 shows a picture of the experimental setup. The batteries have been emulated by a bidirectional DC source/battery emulator model TC.GSS-Bidirectional-DC-PSU from Regatron. The PV array has been emulated by means of a 10 kW PV array simulator TerraSAS ETS1000/10 from Ametek. Three experiments have been carried out. The experimental scenarios are summarized by Table 4. Figures 10 and 11 depict the waveforms of the currents, voltages and powers of the power converters of the DC bus of the MG, corresponding to Figure 10, experiment #1 and Figure 11, experiment #2. Figure 12 correspond to the experiment 3.

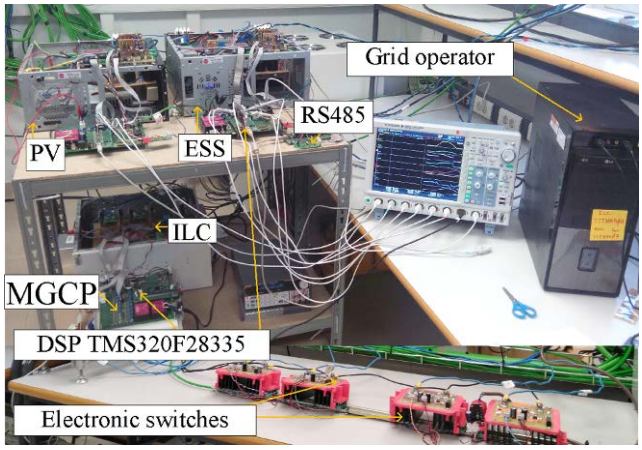

Figure 9. Experimental setup picture.

Experiment #1 and experiment #2 show the behavior of the system with the same change of the irradiation level at the PV source, but with a different SOC of the ESS. The available power injected from the AC bus to the DC bus by the ILC is P_{ILC_DC}=*-1 kW*.

Experiment 1: The ESS is initially at an *SOC≥80%* (charged). In Figure 1 can be observed that the four loads keep connected during the whole experiment. (P_{DC_Load}=*2.4 kW*). The hysteresis level for comparisons with thresholds is: DC_{Load_hyst}=*240 W*.

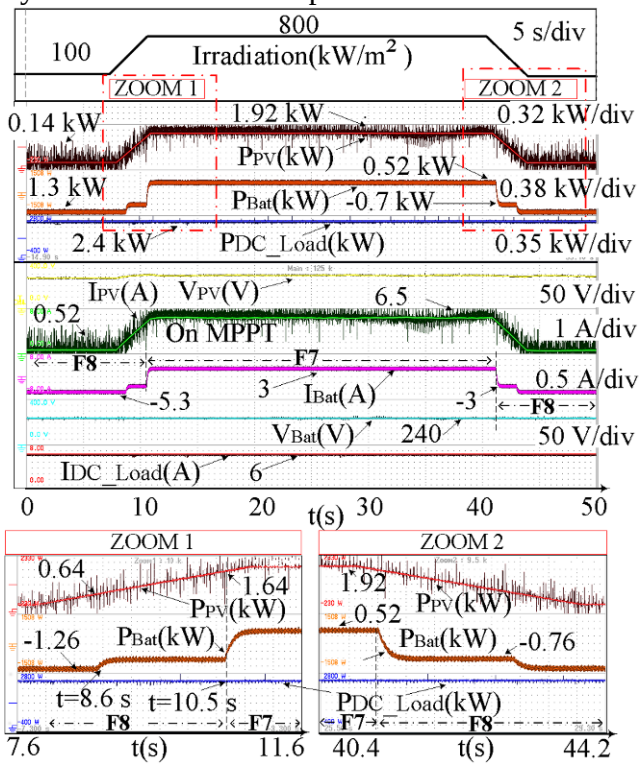

Figure 10. Experiment 1: Evolution of the currents, voltages and the power exchange in the HY MG.

Interval1 1 (0 s<t<8 s): The irradiation level is 100 W/m^2 and the PV source works at its maximum power point (MPP), providing P_{PV}=*140 W* to the DC bus. That irradiation is not enough to feed all the loads. Taking into account that the ESS is charged (*SOC≥80%)* the MGCP transfers the maximum possible power from the AC bus (P_{ILC_DC}=*-1 kW*) to the DC bus through the ILC and applies F8. F8 keeps all the DC loads connected and orders the ESS supplying all the power required by the DC bus, P_{Bat}=*-1.26kW*.

Interval 2 (8 s<t<11 s): The irradiation increases from 100 W/m^2 to 800 W/m^2 en 3 s. The MGCP keeps F8 activated and the power delivered by the ESS can be reduced.
At *t= 8.6 s;* MGCP detects increasing generation, the PV source works at its MPP delivering P_{PV}*=640 W*. The MGCP keeps F8 activated and transfers the maximum possible power from the AC bus (P_{ILC_DC}*=-1 kW*), and keeps all the DC loads connected. ESS supplying all the power required by the DC bus, the power delivered by the ESS is reduced to P_{Bat}*=-0.76 kW*.
At *t= 10.5 s* the PV source works at its MPP delivering P_{PV}*=1640 W*, being P_{ILC_DC}*=-1 kW*. In this moment the MGCP detects that the available power at the DC bus to fed all the DC loads is higher than the hysteresis level (*Cal.1>*DC_{Load_hyst}). The MGCP changes from F8 to F7. F7 forces the ESS to change its operation to energy storage mode, the batteries are charged with a current given by (10). The MGCP changes the setpoint of the ESS charge current I_{Ch_ref}, until the available power generation is stable (At *t=11.6 s,* P_{Bat}*=0.5 kW*).
Experiment 2: The ESS is initially at an *SOC≤20%* (discharged).
Interval 1 (0 s<t <7 s): The irradiation level is 100 W/m^2 and the PV source works at its maximum power point (MPP), providing P_{PV}*=140 W* to the DC bus. That irradiation is not enough to feed all the loads. Considering that the ESS is discharged (*SOC<20%*), the MGCP transfers the maximum possible power from the AC bus (P_{ILC_DC}*=-1 kW*) to the DC bus through the ILC, and applies the load shedding function F11. Taking into account that the available power at the DC bus (1140 W) is not enough to feed two loads, F11 connects only one DC load (600W). The rest of the available power is used for charging the batteries at P_{Bat}*=540 W*.

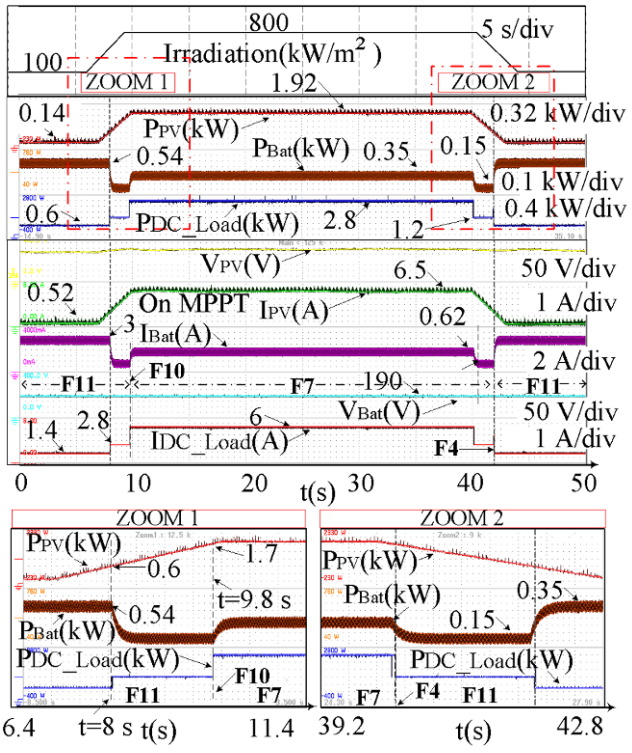

Figure 11. Experiment 2: Evolution of the currents, voltages and the power exchange in the HY MG.

Interval 2 (7 s<t <10 s): The irradiation increases from 100 W/m^2 to 800 W/m^2 in 3 s. The MGCP keeps function F11 activated.
At *t=8 s* the PV source works at its MPP delivering P_{PV}*=600 W*, whereas P_{ILC_DC}*=-1 kW*. At this moment the MGCP detects that the available power at the DC bus taking into account the hysteresis level is enough to feed two of the loads. F11 connects two loads and changes the

setpoint I_{Ch_ref} of the ESS from 2.9 A to 0.78 A, being $P_{Bat}=150\ W$. Note that at $t=8\ s$, after the connection of the two loads, only $|P_{ILC\_DC}| \leq 0.75\ kW$ is taken from the AC bus. This ensures a minimum level of power available in the DC bus.

At t= 9.8 s, the PV source works at its MPP delivering $P_{PV}=1700\ W$, being $P_{ILC\_DC}=-1\ kW$. At this moment the MGCP detects that the available power at the DC bus to feed all the DC loads is greater than the hysteresis level (DC_{Load_hyst}). The MGCP applies function F10 which internally activates the flag $SW_{LoadDC}=ON$. After that the MGCP starts a transition from F10 to F7. F7 connects all the DC loads and changes the setpoint of the ESS, $I_{Ch\_ref}=1.82\ A$ until the available power generation is stable at the instant $t=11.4\ s$, being $P_{Bat}=0.35\ kW$. At $t=9.8\ s$ the MGCP applies function F10 during an execution cycle of the algorithm, i.e. during 73 ms. After that, function F7 is applied. In the zoom areas of figures 10 and 11 the power flow between the generators and the loads can be observed. No oscillations in the transients are observed, which could point out any instability problem.

Experiment 3: The operation functions broadcasted by the MGCP to the MG elements have a communications delay which depends on the RS485 communication system. In the experimental MG the computing time of one operation function and its delay to be broadcasted and processed by one of the elements is lower than 74 ms, as it can be observed in Figure 12.

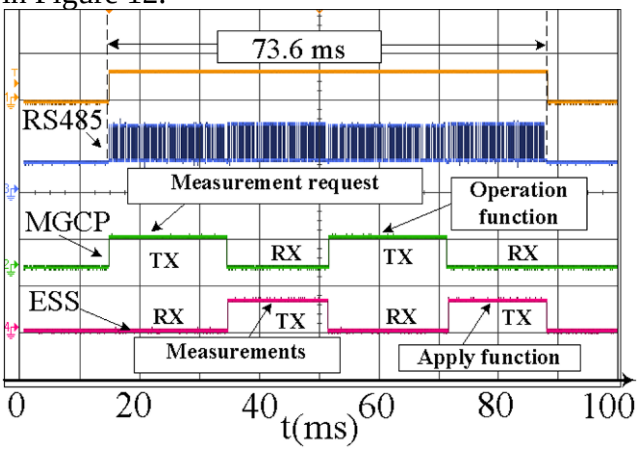

Figure 12. Experiment 3: Computing time of the communication between the MGCP and one of the microgrid elements.

5. Conclusions

A new power management algorithm for the efficient coordination of the power converters composing a hybrid microgrid working in grid-connected mode is presented. The algorithm is programed in a Microgrid Central Processor and it is based on grouping the devices together according to their type: generation, storage, interlinking converter and load. The algorithm selects the suitable configuration of the microgrid among a set of several predefined functions, which establish the configuration of each of the devices in every plausible scenario of the MG. In this paper 12 operations functions have been defined, but that number could be extended. The choice of the functions to be applied depends on the status of the distributed generators, the loads, the energy storage and the energy dispatch limit between the AC and DC buses stablished by the grid operator. The operations functions are the setpoints that define the status of each converter, and are broadcasted by the MGCP through a low bandwidth RS485 communications system. The experimental and simulation results confirm that the proposed power management algorithm allows a suitable power balance among the HY MG devices at changes of the irradiance, of the load and of the state

of charge of the ESS, complying with the power dispatch limit set by the public grid operator.

Acknowledgments

This work has been cofinanced by the Spanish Ministry of Economy and Competitiveness (MINECO) and by the European Regional Development Fund (ERDF) under Grant ENE2015-64087-C2-2.

6. References

[1] Roa-Escalante, Gino de Jesús, Sánchez-Lozano, Juan Miguel, Faxas, Juan-Gabriel, García-Cascales, M. Socorro, Urbina, Antonio. "The effects of photovoltaic electricity injection into microgrids: Combination of Geographical Information Systems, multicriteria decision methods and electronic control modeling", Energy Conversion and Management, Vol. 96, pp. 88-99, 2015.

[2] Ioannis Kougias, Sandor Szabo, Fabio Monforti-Ferrario, Thomas Huld, Katalin Bodis. "A methodology for optimization of the complementarity between small-hydropower plants and solar PV systems". Renewable Energy, Vol. 87, pp. 1023-1030, 2016.

[3] Choudar Adel, Boukhetala Djamel, Barkat c Said, Brucker Jean-Michel. "A local energy management of a hybrid PV-storage based distributed generation for microgrids". Energy Conversion and Management, Vol.90, pp. 21–33, 2015.

[4] Koohi-Kamali Sam, Rahim Nasrudin Abd. "Coordinated control of smart microgrid during and after islanding operation to prevent under frequency load shedding using energy storage system". Energy Conversion and Management, Vol. 127, pp. 623-646, 2016.

[5] Katiraei F, Iravani MR. "Power management strategies for a microgrid with multiple distributed generation units". IEEE Transactions on Power Systems, Vol. 21, pp. 1821–31, 2006.

[6] Manuela Sechilariu, Bao Chao Wang, Fabrice Locment, Antoine Jouglet. "DC microgrid power flow optimization by multi-layer supervision control. Design and experimental validation". Energy Conversion and Management, Vol. 82, pp. 1-10, 2014.

[7]N. Eghtedarpour, E. Farjah. "Control strategy for distributed integration of photovoltaic and energy storage systems in DC micro-grids". Renewable Energy, Vol. 45, pp. 96-110, 2012.

[8] Aushiq Ali Memon, Kimmo Kauhaniemi. "A critical review of AC Microgrid protection issues and available solutions". Electric Power Systems Research; Vol. 129, pp. 23–31, 2015.

[9] Xiong Liu, Peng Wang and Poh Chiang Loh, "A hybrid AC/DC micro-grid", *2010 Conference Proceedings IPEC*, Singapore, pp. 746-751, 2010.

[10] P. Wang, X. Liu, C. Jin, P. Loh and F. Choo, "A hybrid AC/DC micro-grid architecture, operation and control", *2011 IEEE Power and Energy Society General Meeting*, San Diego, CA, pp. 1-8, 2011.

[11] Josep Guerrero, J. V. "Hierarchical Control of Droop-Controlled AC and DC Microgrids. A General Approach Toward Standardization". IEEE TRANSACTIONS ON INDUSTRIAL ELECTRONICS, Vol. 58, pp. 158-172, 2011.

[12] Xiong Liu, Peng Wang, Member and Poh Chiang Loh. "A Hybrid AC/DC Microgrid and Coordination Control". IEEE TRANSACTIONS ON SMART GRID, Vol. 2, pp. 278-286, 2013.

[13] Farzam Nejabatkhah and Yun Wei Li. "Overview of Power Management Strategies of Hybrid AC/DC Microgrid ". IEEE Transactions on Power Electronics, Vol. 30, pp. 7072 – 7089, 2015

[14]Poh Chiang Loh, S. M. "Autonomous Control of Interlinking Converter With Energy Storage in Hybrid AC–DC Microgrid". IEEE TRANSACTIONS ON INDUSTRY APPLICATIONS, Vol. 49, pp. 1374-1376, 2013.

[15] K. De Brabandere, B. Bolsens, J. Van den Keybus, A. Woyte, J. Driesen and R. Belmans, "A Voltage and Frequency Droop Control Method for Parallel Inverters," in *IEEE Transactions on Power Electronics*, vol. 22, no. 4, pp. 1107-1115, July 2007.

[16] Poh Chiang Loh, Ding Li, Yi Kang Chai, and Frede Blaabjerg. "Autonomous Operation of Hybrid Microgrid With AC and DC Subgrids". IEEE TRANSACTIONS ON POWER ELECTRONICS, Vol. 28, pp. 2214-2223, 2013.

[17] F. Luo, K. H. Loo and Y. M. Lai, "A hybrid AC/DC microgrid control scheme with voltage-source inverter-controlled interlinking converters," *2016 18th European Conference on Power Electronics and Applications (EPE'16 ECCE Europe)*, Karlsruhe, pp. 1-8, 2016.

[18]Y. Karimi, J. M. Guerrero and H. Oraee, "Decentralized method for load sharing and power management in a hybrid single/three-phase islanded microgrid consisting of hybrid source PV/battery units," *2016 IEEE Energy Conversion Congress and Exposition (ECCE)*, Milwaukee, WI, USA, pp. 1-8, 2016.

[19]M. A. Hasan, N. K. Vemula and S. K. Parida, "Cost based dynamic load dispatch for an autonomous parallel converter hybrid AC-DC microgrid," *2016 National Power Systems Conference (NPSC)*, Bhubaneswar, India, pp. 1-5, 2016.
[20] MODBUS APPLICATION PROTOCOL SPECIFICATION V1.1b. http://www.modbus.org/docs/Modbus_Application_Protocol_V1_1b.pdf
[21] S. Kenner, R. Thaler, M. Kucera, K. Volbert and T. Waas, "Smart Grid architecture for monitoring and analyzing, including modbus and REST performance comparison," 2015 12th International Workshop on Intelligent Solutions in Embedded Systems (WISES), Ancona, pp. 91-96, 2015.
[22] PowerSim. PSIM7.0. 2006.

Index of Figures

Figure 1. Conceptual scheme of the hybrid microgrid under study.

Figure 2. Power flow scenarios between the grid and the HY MG: (a) $P_{Grid}<0$, power flow from the Grid to HY MG and (b) $P_{Grid}>0$, power flow from the HY MG to Grid.

Figure 3. Power dispatch inside the HY MG after applying the operation functions: (a) Function 3, (b) Function 8, (c) Function 10 and (d) Function 11.

Figure 4. DC load shedding function.

Figure 5. Power management algorithm of the HY MG.

Figure 6. Evolution of the currents of the HY MG and of the SOC of the batteries.

Figure 7. Evolution of the power exchange at the HY MG and irradiation.

Figure 8. Detail of the strongest transient of I_{ILC_AC}, V_{Grid}, V_{DC} and P_{ILC_AC}, which takes place in interval 7.

Figure 9. Experimental setup picture.

Figure 10. Experiment 1: Evolution of the currents, voltages and the power exchange in the HY MG.

Figure 11. Experiment 2: Evolution of the currents, voltages and the power exchange in the HY MG.

Figure 12. Experiment 3: Computing time of the communication between the MGCP and one of the microgrid elements.

Index of Tables

Table 2. Communication parameters of the system.

Table 2. Nomenclature.

Table 3. Characteristics of the power converters of the HY MG.

Table 4. Possible scenarios of the HY MG.